A Comparison of Methodologies for Representing Path Effects on Regional P/S Discriminants

Article *in* Bulletin of the Seismological Society of America · April 1999

CITATIONS
35

READS
71

5 authors, including:

Arthur Rodgers
Lawrence Livermore National Laboratory
219 PUBLICATIONS **1,984** CITATIONS
SEE PROFILE

William Walter
Lawrence Livermore National Laboratory
209 PUBLICATIONS **3,345** CITATIONS
SEE PROFILE

S. C. Myers
Lawrence Livermore National Laboratory
128 PUBLICATIONS **2,470** CITATIONS
SEE PROFILE

Thorne Lay
University of California, Santa Cruz
518 PUBLICATIONS **16,936** CITATIONS
SEE PROFILE

Bulletin of the Seismological Society of America, 89, 2, pp. 394–408, April 1999

A Comparison of Methodologies for Representing Path Effects on Regional *P/S* Discriminants

by Arthur J. Rodgers, William R. Walter, Craig A. Schultz, Stephen C. Myers, and Thorne Lay

Abstract Short-period regional *P/S* amplitude ratios hold much promise for discriminating low-magnitude explosions from earthquakes in a Comprehensive Test Ban Treaty (CTBT) monitoring context. However, propagation path effects lead to variability in regional-phase amplitudes that, if not accounted for, can reduce or eliminate the ability of *P/S* ratios to identify the seismic source. Here we compare four different methodologies that account for the effect of heterogeneous structure on *P/S* amplitude variance: (1) distance corrections, (2) path-specific crustal waveguide parameter regressions, (3) cap averaging (running mean smoothing), and (4) kriging. The predictability of each method is established by cross-validation (leave-one-out) analysis. We apply these techniques to *Pn/Lg*, *Pg/Lg*, and *Pn/Sn* observations in three frequency bands from 0.75 to 6.0 Hz at station ABKT (Alibek, Turkmenistan), site of a primary station of the International Monitoring System (IMS). Paths to ABKT sample diverse crustal structures (e.g., various topographic, sedimentary, and geologic structures), leading to great variability in the observed *P/S* amplitude ratios. For these data to be useful for isolating source characteristics, the scatter needs to be reduced by accounting for the path effects, and the resulting distribution needs to be Gaussian for most existing spatial interpolation and discrimination strategies to have valid application. Each method reduces the scatter of the *P/S* amplitude measurements with varying degrees of success; however, kriging has the distinct advantages of providing the greatest variance reduction and a continuous correction surface with an estimate of the model uncertainty. The largest reductions in scatter are found for the lowest frequency *P/S* ratios (<3.0 Hz).

Introduction

Short-period regional seismic phases will play an important role in monitoring the Comprehensive Test Ban Treaty (CTBT) for events with body-wave magnitudes, m_b, less than about 4.0. Because signal to noise is generally small for low-magnitude events at teleseismic distances (distances greater than about 1500 km), discrimination strategies based on M_S:m_b, radiation pattern, and source depth may not provide sufficiently reliable source characterization (e.g., Blandford, 1981; Pomeroy *et al.*, 1982; National Research Council, 1997). Short-period *P/S* discriminants, for example, *Pn/Lg*, *Pg/Lg*, and *Pn/Sn* amplitude ratios, have been shown to be effective at discriminating earthquakes and explosions at regional distances and small magnitudes (Bennett and Murphy, 1986; Taylor *et al.*, 1989; Baumgardt and Young, 1990; Kim *et al.*, 1993; Walter *et al.*, 1995; Taylor, 1996; Hartse *et al.*, 1997). However, the travel times and amplitudes of regional phases vary greatly due to acute sensitivity to highly heterogeneous lithospheric structure. An understanding of and correction for variations in these *P/S* amplitude ratios is necessary before they can be used reliably as discriminants. Many of the regional *P/S* discrimination studies to date have relied on simple one-dimensional geometric spreading and attenuation corrections. However, in complex regions, these simple corrections are recognized as inadequate. There have been a number of recent empirical studies to correct regional phases for path effects. In this article, we systematically and objectively compare the four most promising techniques using a common data set.

For many years, observations of short-period *Sn* and *Lg* amplitudes have been qualitatively characterized in terms of spatially varying propagation efficiency. For example, studies by Kadinsky-Cade *et al.* (1981) and Rodgers *et al.* (1997a) report regional variations in short-period (frequencies 0.5 to 5.0 Hz) *Sn* and *Lg* amplitudes in the Middle East. These studies report strong attenuation or inefficient propagation of *Sn* for the Turkish–Iranian plateau and blockage of *Lg* by remnant oceanic crust (e.g., the southern Caspian and Black Seas). Attenuation of *Lg* is higher within the Turkish–Iranian plateau than in more tectonically stable regions of Eurasia (Mitchell *et al.*, 1997). Inefficient propagation of

Sn is associated with high elevations of the Turkish–Iranian plateau, low *Pn* velocities (Hearn and Ni, 1994), and recent volcanism. Seismic source discrimination and monitoring of the CTBT will require quantitative representation of regional-phase amplitude behavior using modern broadband data and identification of phase blockages.

Recent investigations have sought to understand the quantitative behavior of short-period regional *P/S* amplitude ratios in terms of crustal wave-guide structure. These studies establish empirical correlations between *P/S* amplitude behavior and along-path topographic, bathymetric, sediment, and crustal structures (Baumgardt, 1990; Zhang and Lay, 1994a,b; Zhang *et al.*, 1996; Baumgardt, 1996; Baumgardt and Schneider, 1997; Hartse *et al.*, 1998). Studies by Zhang *et al.* (1994), Fan and Lay (1998a,b), and Rodgers *et al.* (1997b) investigate crustal wave-guide effects using multivariate regression analysis. Multivariate regressions find linear combinations of propagation path parameters that best describe the observed amplitude ratio data. A drawback of this method is that models of crustal and sediment thickness are poorly known. Fan and Lay (1998a) found that the most important crustal wave-guide parameters controlling low-frequency (<3.0 Hz) *Pg/Lg* behavior in western China are distance, mean elevation, mean crustal thickness, and mean sediment thickness on each path. These results show that the scatter in regional *P/S* discriminants can be significantly reduced with simple empirical models (variance reductions of 75% have been obtained). Using short-period waveform data recorded at the Iran Long-Period Array (ILPA) for paths propagating primarily within the Iranian plateau, Baumgardt and Schneider (1997) showed that average basement depth is an important factor influencing *Pn/Lg* amplitude ratios in Iran. This conclusion was also reached by multivariate analysis of *P/S* ratios observed at station ABKT (Rodgers *et al.*, 1997b). Studies of crustal wave-guide effects on regional amplitude ratios will hopefully lead to a physical basis for understanding short-period *P/S* behavior and can be used to guide theoretical modeling of short-period regional seismic-wave propagation. Because the regression coefficients of along path crustal parameters that reduce the *P/S* ratio variance change from region to region and a predictable physical basis for these effects remains to be established, it is not clear if these regressions will be universally effective at reducing the scatter of *P/S* ratios.

Two techniques for spatially averaging data have been recently applied to station-based seismic observations. First, an effort to represent short-period regional-phase amplitude behavior is reported by Phillips *et al.* (1998). They used a cap-averaging scheme (running mean smoothing) to produce maps of source- and distance-corrected absolute amplitudes of each regional phase. Cap averaging finds the average value within a circular area of a specified radius (cap) and projects the value to the center of the circle. This technique results in a continuous correction surface where there is sufficient data coverage to estimate an average value. However, gaps exist in regions where data are sparse or absent. This procedure requires the selection of a cap size (radius) and minimum number sampling per cap. These parameters can strongly impact the resulting surface. Using this technique, Phillips *et al.* (1998) obtained variance reductions of as much as 57% for low-frequency *P/Lg* amplitude ratios observed in China. The second spatial averaging technique has been introduced by Schultz *et al.* (1998). This study modifies the geostatistical technique of kriging to compute correction surfaces for regional *P*-wave travel-time residuals. Modified kriging defines a continuous correction surface using the observed data and uncertainty along with parameters that model the spatial correlation and expected background values. The modifications of the kriging algorithm by Schultz *et al.* (1998) account for variable data uncertainties and force the surface to return to an *a priori* background model in regions of sparse coverage to remove unphysical extrapolation artifacts. We found the modified kriging technique to have several distinct advantages over other representation methods.

This article explores the effectiveness of various methodologies for representing the variability of short-period regional *P/S* amplitude ratios observed at station ABKT (Alibek, Turkmenistan). For real-time monitoring of the CTBT, there are several issues to consider. First, the path propagation amplitude correction model must successfully represent the input data. A certain problem with this empirical approach is that we have little or no observations for aseismic regions, thus we cannot calibrate the earthquake behavior of these regions. Another important issue is that corrections for path propagation effects on regional-phase amplitudes should vary smoothly and continuously as a function of location. This is required because event locations, especially regional locations, can have uncertainties on the order of 20 to 30 km. It is highly undesirable for corrections to change rapidly with position or for the correction to be undefined within the error ellipse of the estimated location. Finally, it is important for any amplitude correction to have a realistic uncertainty. For example, if a suspicious event occurs and its path propagation amplitude correction has a large uncertainty, then this needs to be included in the event identification process. A similar situation arises in event location as well—path-specific travel-time corrections can be applied and their uncertainty can be carried through the event location estimation process and mapped into the location uncertainty.

Station ABKT is located on the northern flank of the Kopet Dagh Mountains near the major tectonic boundary separating the Iranian plateau to the south from the Kazakh platform to the north (Fig. 1, an event list can be obtained from the first author). The *P/S* amplitude ratios observed at ABKT show strong spatial variability, presumably related to topographic, geologic, tectonic, and crustal wave-guide structure. Thus, these *P/S* amplitude ratio data are well suited for a comparison of representation methodologies. Station ABKT is near the site of the planned International Monitoring System (IMS) primary array GEYT. Thus, calibration of

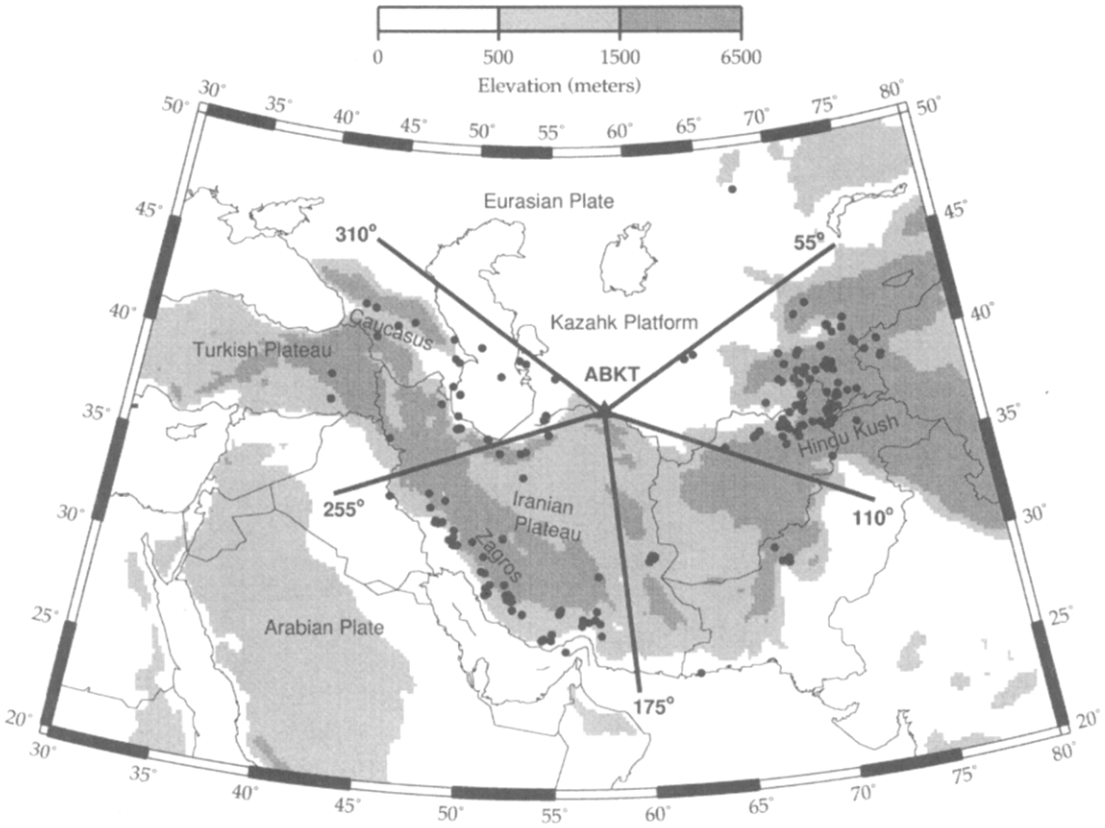

Figure 1. Locations of earthquakes (circles) and station ABKT (triangle), along with topography and regional tectonic features. Thick lines represent the boundaries used to subdivide the data by azimuthal sector.

regional-phase amplitudes at ABKT may be helpful for future calibration of GEYT.

Regional Waveform Data at ABKT and *P/S* Amplitude Ratio Measurements

Broadband waveform data (20 samples/sec) recorded at station ABKT were requested from the Incorporated Research Institutions for Seismology–Data Management Center (IRIS-DMC). Event parameters were taken from the National Earthquake Information Center–Preliminary Determination of Epicenters (NEIC-PDE). Because we are most interested in crustal earthquakes and phases, the reported depths were restricted to be less than 50 km. Distances were limited to 200 to 1500 km to avoid misidentifying *Pg* as *Pn* at close range and upper mantle triplications at far regional distances. The reported body-wave magnitudes of the events used span the range 3.9 to 6.1. All waveforms were previewed. In this study, we considered only vertical-component data. A first-arriving *P* wave was picked. Noisy data and data with interfering events were immediately discarded. Previewing resulted in nearly 200 regional events recorded at ABKT for the years 1993 to 1996. These events are plotted in Figure 1, along with the station location, topography, and major tectonic features.

Regional-phase amplitude ratios and signal-to-noise ratios were measured for these data in three frequency bands (0.75 to 1.5, 1.5 to 3.0, and 3.0 to 6.0 Hz). Phases were isolated with the following group velocities: *Pn* 8.0 to 7.6 km/sec, *Pg* 6.5 to 5.5 km/sec, *Sn* 4.6 to 4.0 km/sec, and *Lg* 3.6 to 3.0 km/sec. Noise measurements were taken for a window of length equal to the *Pn*, *Pg*, or *Lg* window ending 5 sec before the first-arriving *P* wave. Example seismograms showing the variability of *Sn* and *Lg* amplitudes can be seen in Rodgers *et al.* (1997a). To account for possible location and origin time errors, time windows were shifted such that the *Pn* arrival came in at 8.0 km/sec. A *Pn* tomography study by Hearn and Ni (1994) reports that 8.0 km/sec is an appropriate average value for the region. If this time shift was greater than 15 sec, the waveform was discarded. This was done to avoid gross location and origin time errors and their effects on windowing the regional phases. These origin time shifts were typically smaller than 10 sec. Given the uncertainties in event location, depth, and origin time, these window shifts isolate the first-arriving *P* wave in a consistent fashion. To the extent that our group velocity windows are

appropriate, the later-arriving phases should be windowed better after applying these window shifts. For distances greater than a few hundred kilometers, *Pg* is often difficult to pick because it is not a distinct phase in a high passed seismogram. The energy arriving in the *Pg* window contains crustally trapped *P*-wave energy. *Pg/Lg* amplitude ratios have been shown to be effective at discriminating earthquakes and explosions for distances out to 1300 km in the Basin and Range Province of the western United States (Taylor, 1996).

Absolute amplitudes within each band were measured in the frequency domain by computing the log-10 mean spectral amplitude of each individual phase from the smoothed broadband instrument-deconvolved displacement spectrum, similar to Walter *et al.* (1995) and Taylor (1996). Ratios were formed from the individual spectral amplitudes. Rodgers *et al.* (1997c) showed that time-domain and frequency-domain measurements of regional-phase amplitude ratios are similar for frequencies less than 3.0 Hz. It is not known if one amplitude measurement method, time or frequency domain, discriminates better. We have recently shown that time-domain rms and frequency-domain measurements of regional amplitude ratios result in about the same discrimination performance of earthquake and explosion data from the Nevada Test Site.

Phase amplitudes were compared to pre-*Pn* background noise to form signal-to-noise ratios for each phase and frequency band. Only data for which the signal-to-noise ratio was greater than 2:1 for each phase and frequency band were used in the analysis. Because the signal-to-noise ratio was measured for later-arriving phases by comparing *S*-wave amplitudes to pre-*Pn* noise (rather than prephase noise), we could be including data where *Sn* and *Lg* are very weak. This is especially true for the higher frequencies. Maps of the *Pn/Lg, Pg/Lg,* and *Pn/Sn* amplitude ratios are plotted in Figure 2. The behavior of all three *P/S* ratios is quite similar. These maps show that the *P/S* ratios from the Hindu Kush region are often low (indicating strong *S*-wave energy), and the *P/S* ratios from the Zagros region are typically high (indicating weak *S*-wave energy). Note that due to poor signal-to-noise ratio, many events from the Zagros are discarded for the highest frequency band.

Distance Corrections

Following Taylor and Hartse (1998), the instrument-corrected amplitude of a regional phase, $A(f)$, can be represented in the frequency domain as

$$A(f,\Delta) = S(f)\ G(\Delta)\ Q(f),$$

where f is frequency, Δ is the epicentral distance, $S(f)$ is the source spectrum, $G(\Delta)$ is the geometric spreading factor, and $Q(f)$ is the attenuation operator. Geometric spreading does not depend on frequency and is simply dependent on a power of the distance. For a fixed frequency band, the attenuation operator depends only on distance. Forming the *P/S* amplitude ratio within the same frequency band explicitly cancels the source spectrum and yields a form that depends on the differential effects of *P*- and *S*-wave geometric spreading and attenuation. For the amplitude ratios, it is generally assumed that source radiation, depth, and site effects cancel. Strictly speaking, this is probably not true, but there is no way to account for these because the effects of source depth and focal mechanism on short-period regional phases and the depths and mechanisms themselves are largely unknown. If there is sufficient sampling of depths and focal mechanisms, then hopefully these effects will average out. Scattering of high-frequency energy probably reduces the effects of depth and mechanism on regional-phase amplitudes. We plotted the *P/S* ratios versus the PDE m_b and found no significant trend with magnitude. This indicates that source-scaling and corner frequency effects are eliminated by forming the *P/S* ratio within the same frequency band. Thus, under the above-stated assumptions, for a region where the elastic and anelastic structure is homogeneous, the amplitude ratio behavior for regional earthquakes should vary most strongly with distance as a result of geometric spreading and attenuation. In the following, we model the *P/S* amplitude ratios by their linear trend with distance.

The $\log_{10}[Pn/Lg]$ amplitude ratios are plotted versus distance and fit to a linear regression in Figure 3a. The data are very scattered, and the linear correlations of these data with distance are rather weak. It is apparent from the maps of the *P/S* ratios (Fig. 2) that paths coming from the Zagros Mountains result in higher *P/S* ratios than those emerging from the Hindu Kush. Because these source regions are at approximately the same distance from ABKT, this behavior must result from path effects that cannot be described by a single one-dimensional distance correction.

When ratios are subdivided by sectoring the major source regions by backazimuth from the station as drawn in Figure 1, the resulting distance corrections are much more strongly correlated with distance, and variance reductions are greater for the subdivided data relative to the entire data set (Rodgers *et al.,* 1997d). In Figures 3b, 3c, and 3d, the linear regressions of $\log_{10}[Pn/Lg]$ with distance are shown when the backazimuths are limited to isolate distinct source regions with differing *P/S* amplitude behavior (see Fig. 1). The correlations shown in Figure 3b, 3c, and 3d are much stronger than those seen in Figure 3a. This is most clear for the lowest frequency band (0.75 to 1.5 Hz). Furthermore, the slopes and intercept values are different for the Hindu Kush and Zagros regions, indicating that the propagation effects are different for these two source regions. The standard error about the regression fit (*se*) is smaller for the sectorized data sets than for the entire data set, indicating that the scatter can be more favorably reduced by subdividing the data by source region.

The effectiveness of the distance corrections on *Pn/Lg* ratios can be seen from the cross-validation statistics compiled in Table 1. Cross-validation measures the effectiveness

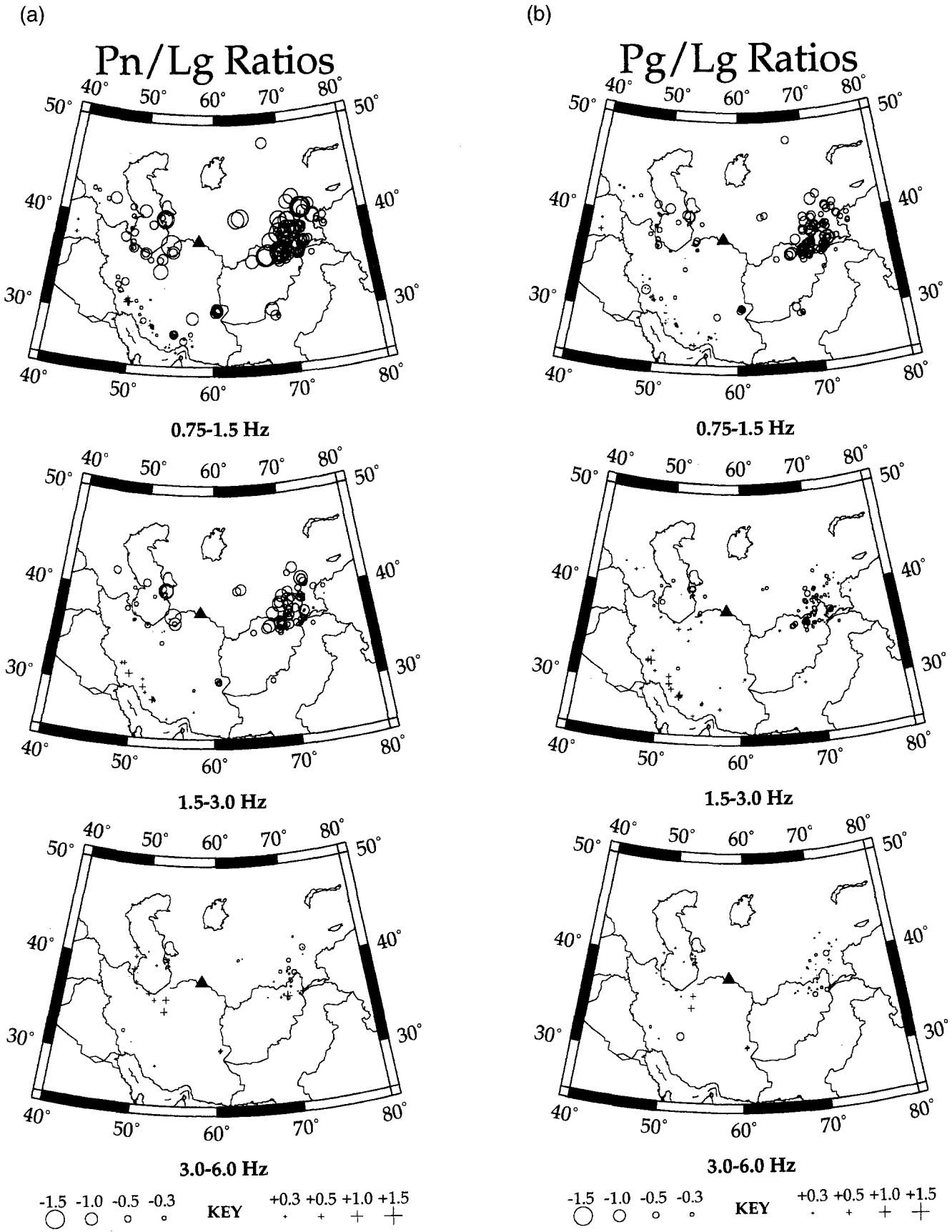

Figure 2. Maps of the $\log_{10}$ (a) *Pn/Lg*, (b) *Pg/Lg*, and (c) *Pn/Sn* amplitude ratios observed at ABKT (plotted at the event location) for three frequency bands.

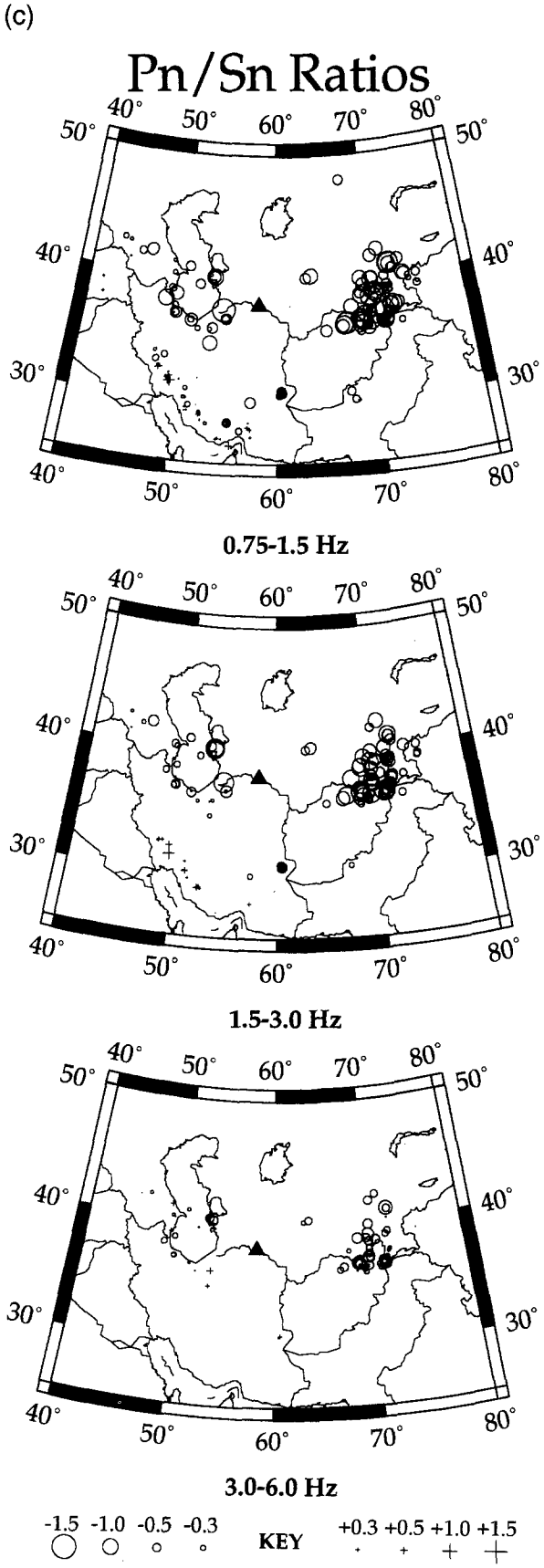

Figure 2. Continued.

of a correction in a realistic manner by removing an observation and using all the remaining data to estimate a correction for the left out observation. This method insures that the correction for any single data point is not influenced by the point itself. Distance corrections based on data for all azimuths do not model much of the scatter (ALL $\Delta\sigma_1 = -3.9\%$ for the 0.75 to 1.5 Hz band). However, rms reductions obtained by simply subdividing the data by backazimuth, $\Delta\sigma_1$, are greater (7 to 30%). When the sectorized distance corrections are applied to the entire data set, greater rms reductions, $\Delta\sigma_2$, are obtained (39.0% for 0.75 to 1.5 Hz, 26.4% for 1.5 to 3.0 Hz). The distributions of the raw and cross-validated *Pn/Lg* ratios for the frequency band 0.75 to 1.5 Hz are shown in Figures 4a and 4b, respectively. Note that not all data were included in the sectorization. The cross-validated data are much less scattered and more normally distributed relative to the raw data. The case of station ABKT is unique in that the station is situated near a major tectonic and topographic boundary and the event-station paths lend themselves to subdivision by azimuthal sectors. This is certainly not the case for all stations.

Path-Specific Crustal Wave-Guide Corrections

In recent years, several studies have explored the correlations between parameters that characterize the path-specific crustal wave-guide and regional-phase amplitude ratios (e.g., Baumgardt, 1990; Zhang and Lay, 1994a,b; Zhang *et al.*, 1996; Baumgardt, 1996; Baumgardt and Schneider, 1997; Rodgers *et al.*, 1997b; Fan and Lay, 1998a,b; Hartse *et al.*, 1998). These studies report that the scatter in regional-phase amplitudes can be reduced by applying either univariate or multivariate path corrections based on crustal wave-guide parameters. The most important wave-guide parameters vary with data set and region, but generally, the strongest correlations are found for distance, mean elevation, mean sediment thickness, and mean crustal thickness. An important conclusion from these studies is that often the observed scatter is reduced more by a crustal wave-guide parameter (such as mean elevation, crustal thickness, or sediment thickness) than by a standard one-dimensional distance correction. This suggests that path propagation effects in regions of crustal wave-guide variability are more important than distance effects alone. These regressions typically result in greater variance reductions for the more variable low-frequency (<3.0 Hz) ratios. Detailed statistical analysis of crustal wave-guide effects on regional *P/S* ratios observed at station ABKT is described in a previous report (Rodgers *et al.*, 1997b). That study reports that distance, mean elevation, and mean sediment thickness are the most important single factors impacting the *Pn/Lg* and *Pn/Sn* ratios observed at ABKT for frequencies below 3.0 Hz. Regression on these three parameters (plus a constant) lead to rms reductions of up to 30%. Multivariate regressions that add rms elevation and mean crustal thickness to these parameters can improve the rms reduction by a few percent over that which is

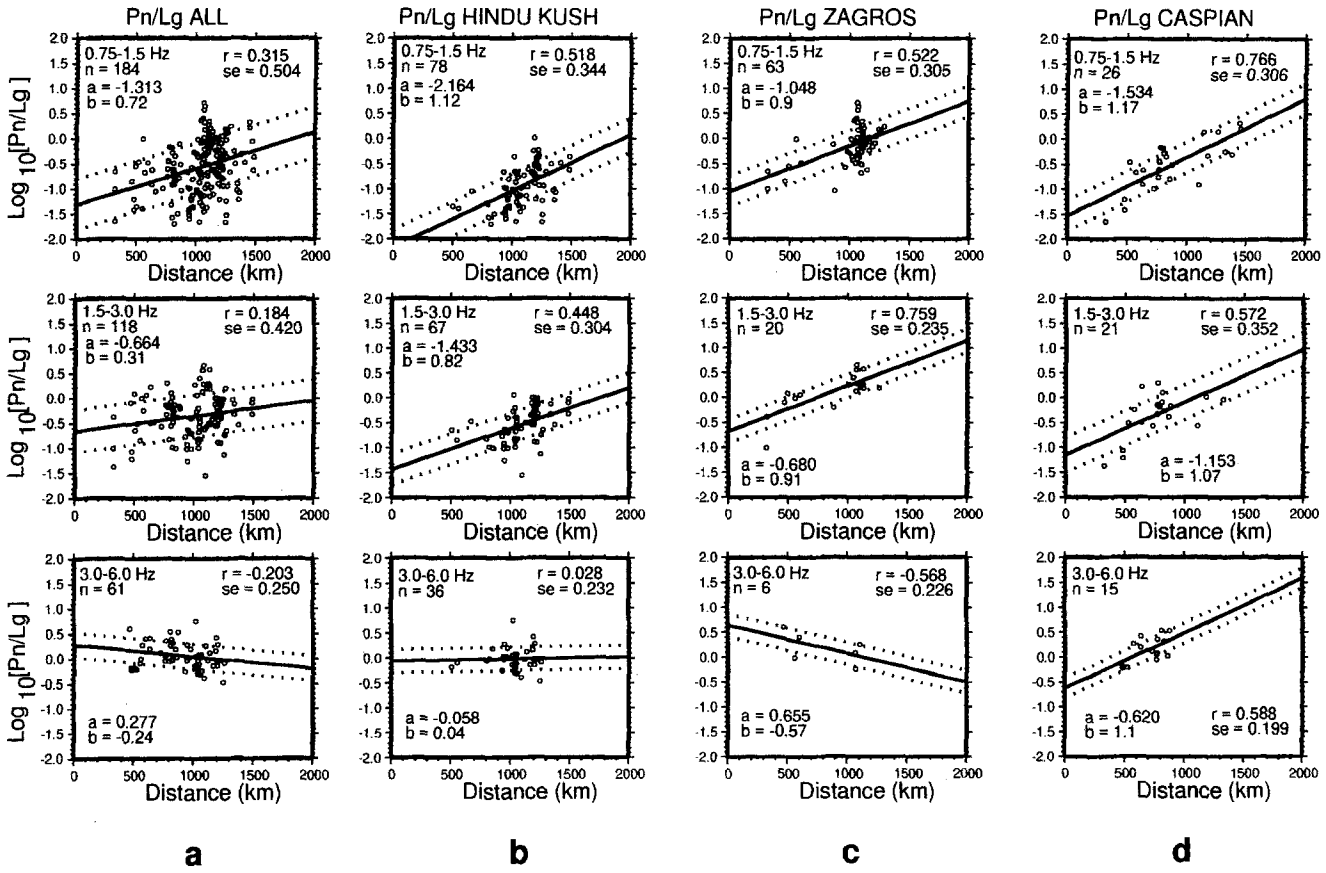

Figure 3. $\text{Log}_{10}[Pn/Lg]$ amplitude ratios versus distance for (*top*) 0.75 to 1.5 Hz, (*middle*) 1.5 to 3.0 Hz, and (*bottom*) 3.0 to 6.0 Hz. The regression fit (solid) and 1-σ uncertainty (dashed) are also plotted. (a) Ratios from all backazimuths; (b) ratios from the Hindu Kush, backazimuths: 55° to 110°; (c) ratios from the Zagros, backazimuths: 175° to 255°; and (d) ratios from the Caspian, backazimuths 255° to 310°. In each panel, the regression statistics are given: number of data, *n*; linear correlation, *r*; standard error about the regression, *se*; the regression parameters intercept, *a*; and slope, *b*.

achieved with distance, mean elevation, and mean sediment thickness.

Analysis of crustal wave-guide effects on *P/S* ratios is repeated for the current data set to evaluate the effectiveness of the path parameter regression method relative to other methods. Crustal wave-guide models are exactly the same as those presented in Fan and Lay (1998a,b) and Rodgers *et al.* (1998b). Topography was taken from the global topography model GTOPO30. This model represents continental surface elevation on a 30-sec (0.93-km) grid. Sediment thickness (basement depth) and crustal thickness (Moho depth) were taken from maps produced by the Former Soviet Union Institute of Physics of the Earth (IPE) (Kunin and Sheykh-Zade, 1983; Kunin, 1987). These models were digitized and gridded (10 km) by Seber *et al.* (1997). Sediments are extremely thick in the southern Caspian basin (>30 km) and moderately thick in the Mesopotamian foredeep (>10 km) and the basins in around Iran. Crustal thickness does not vary greatly for the paths to ABKT (mean values are typically 40 to 50 km). The accuracy of these models is certainly debatable; however, because we are only interested in average values and not point-wise values or gradients, the IPE basement and Moho depth models are probably adequate.

Univariate regressions of the $\log_{10}[Pn/Lg]$ amplitude ratios on mean elevation and mean sediment thickness are shown in Figures 5a and 5b, respectively. Linear correlations involving the *Pn/Lg* ratios (<3.0 Hz) are stronger for mean elevation and mean basement depth than for distance, and the scatter after the trends are removed is smaller. It is interesting to note that the *Pn/Lg* ratios have a negative trend with mean sediment depth, indicating that *Lg* is stronger than *Pn* for paths with thicker sediment on average. For the ABKT data set, paths from the Hindu Kush pass through the thick sedimentary cover of the Turkmen Basin while paths from the Zagros pass through several smaller sedimentary basins. This observation may support the idea that changes in sedimentary basin depth can weaken *Lg* amplitudes as suggested by Baumgardt and Schneider (1997). The correlations in Figure 5 are weak for higher frequency ratios, possibly

Table 1
Statistics of Cross-Validated Data Using Distance Corrections

Pn/Lg 0.75–1.5 Hz

Data Set	Number	Mean	σ	$\Delta\sigma_1$	$\Delta\sigma_2$
ALL data	167	−0.5553	0.5490	—	—
ALL c-v	167	0.0000	0.5277	−3.9%	−39.0%
HINDU KUSH data	78	−0.9129	0.4018	—	—
HINDU KUSH c-v	78	0.0003	0.3514	−12.5%	—
ZAGROS data	63	−0.1066	0.3576	—	—
ZAGROS c-v	63	−0.0003	0.3133	−12.4%	—
CASPIAN data	26	−0.5122	0.4760	—	—
CASPIAN c-v	26	−0.0043	0.3333	−30.0%	—

Pn/Lg 1.5–3.0 Hz

Data Set	Number	Mean	σ	$\Delta\sigma_1$	$\Delta\sigma_2$
ALL data	108	−0.3673	0.4425	—	—
ALL c-v	108	−0.0008	0.4418	−0.2%	−26.4%
HINDU KUSH data	67	−0.5284	0.3396	—	—
HINDU KUSH c-v	67	0.0015	0.3128	−7.9%	—
ZAGROS data	20	0.1415	0.3614	—	—
ZAGROS c-v	20	−0.0049	0.2762	−23.6%	—
CASPIAN data	21	−0.3380	0.4296	—	—
CASPIAN c-v	21	−0.0197	0.3999	−6.9%	—

σ = root mean square, rms.
$\Delta\sigma_1$ = rms reduction of cross-validated data relative to sectorized data.
$\Delta\sigma_2$ = rms reduction of cross-validated sectorized data relative to ALL data.
c-v = cross-validated data set using leave-one-out analysis.

because many high-frequency data are lost due to low signal-to-noise ratio and the variability of the path sampling is diminished. We regressed the low-frequency *P/S* amplitude ratios on five path parameters (distance, mean elevation, rms elevation, mean crustal thickness, and mean sediment thickness) plus a constant. The effectiveness of these regressions can be seen in the cross-validation statistics compiled in Table 2. Rms reductions on the order of 25% are obtained for the low-frequency *P/S* ratios using the path parameter regression method. The distributions of the raw and corrected ratios using cross-validation are plotted in Figures 4a and 4c, respectively. Although the scatter of the raw data is diminished, the distribution of the corrected data appears to be bimodal. The available crustal wave-guide characterizations appear not to capture the basic distinctions that allow the azimuthal sectorization to further reduce the scatter in Figure 4b.

Correction Surfaces by Cap Averaging

In a recent study, Phillips *et al.* (1998) used a spatial averaging technique to construct geographic patterns of source- and distance-corrected absolute amplitudes of regional phases. These patterns (correction surfaces) were derived by computing the moving average (cap average) of the $\log_{10}$ amplitude residual observed at a single station and projected to the event location. When more than a specified minimum number of observations fall within a specified radius, the data are averaged. Although they cap averaged the absolute amplitude data, forming corrections for amplitude ratios resulted in variance reductions of as much as 57% for the low-frequency *P/Lg* data. Using the same amplitude ratio data as that presented in previous sections, we computed correction surfaces using the cap-average method. The data mean was removed before the correction surface was computed. We chose to use a cap radius of 2.5° (similar to Phillips *et al.,* 1998) and required there to be five or more observations within each cap. The choice of the cap size and minimum number of data per cap can strongly impact the resulting correction surface. For example, if the region is uniformly sampled and the values vary slowly across the region, then a small cap size may be appropriate to model the data variability. However, if the region is unevenly sampled (as is the usual case for seismic data), then it may not be possible to determine the true rate of spatial variability (correlation length). In such a case, if one chooses the cap size or the minimum number of data per cap to be small, then there will be gaps in the surface. If these parameters are made too large, then the spatial variability of the data might not be well represented.

Figure 6a shows the cap-averaged *Pn/Lg* ratios in the 0.75 to 1.5 Hz pass band. The different mean values of the Hindu Kush and Zagros source regions are clear. These regions can be well defined by the 2.5° cap, and thus the cap-averaging method results in a surface that represents these features; however, smaller-scale variability is not matched. An obvious problem of the cap-average method is that the surface can only be defined where there are a sufficient number of observations. Where there are observations but no defined surface, it was not possible to compute a mean value using the stated cap size and minimum number sampling. The predictability of this method can be seen from the histogram plotted in Figure 6d. The scatter of the corrected data is reduced by 37.1% and the distribution appears to be closer to a Gaussian distribution than the input ratios (Fig. 6a). Note that 24 observations (184 to 160) that were in the input data set were not corrected because of gaps in the cap-averaged surface.

Correction Surfaces by Modified Kriging

Kriging is a minimum variance, linear estimation technique that models nonuniformly distributed data as a continuous surface with uncertainty estimates. Recent modification of the kriging algorithm and application to seismic travel times by Schultz *et al.* (1998) make it possible for this technique to be applied to other types of seismic observables in a CTBT monitoring context. There are several distinct features of the modified kriging technique. First, a continuous smooth surface is generated for a region of arbitrary size. Second, the observations and associated uncertainties drive the solution so that in areas of dense data coverage, the resulting surface is close to the local average of the observa-

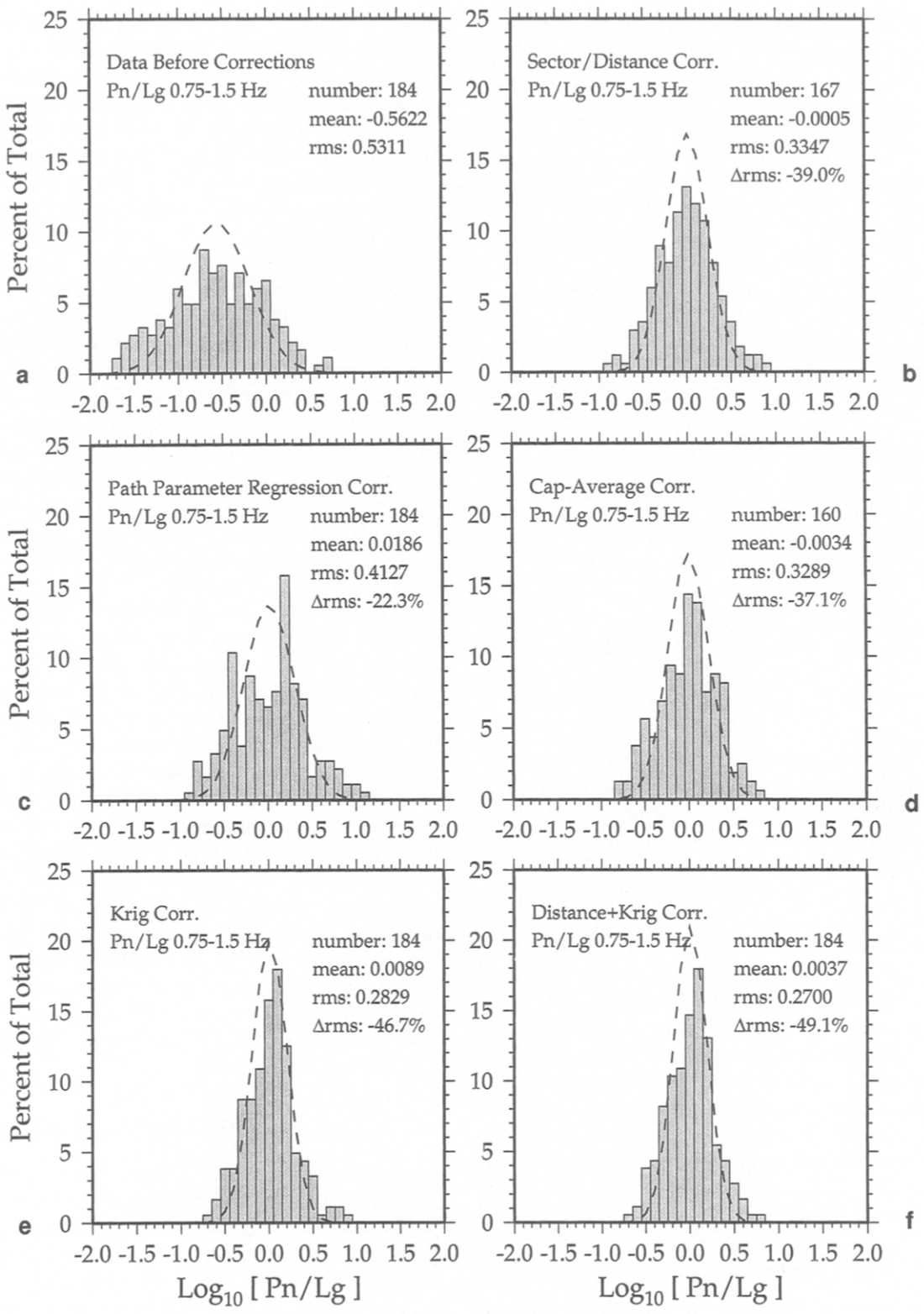

Figure 4. Histograms of the *Pn/Lg* ratios (0.75 to 1.5 Hz) (a) before and (b to f) after the various corrections for path effects were made. All distributions for data sets after corrections were removed were computed by cross-validation: (b) sectorized distance corrections; (c) multivariate path parameter regression using distance, mean elevation, rms elevation, mean crustal thickness, and mean sediment thickness; (d) cap averaging; (e) kriging, and (f) kriging after distance trend was removed. A Gaussian with equal mean and variance is plotted in each panel (dashed line) for comparison.

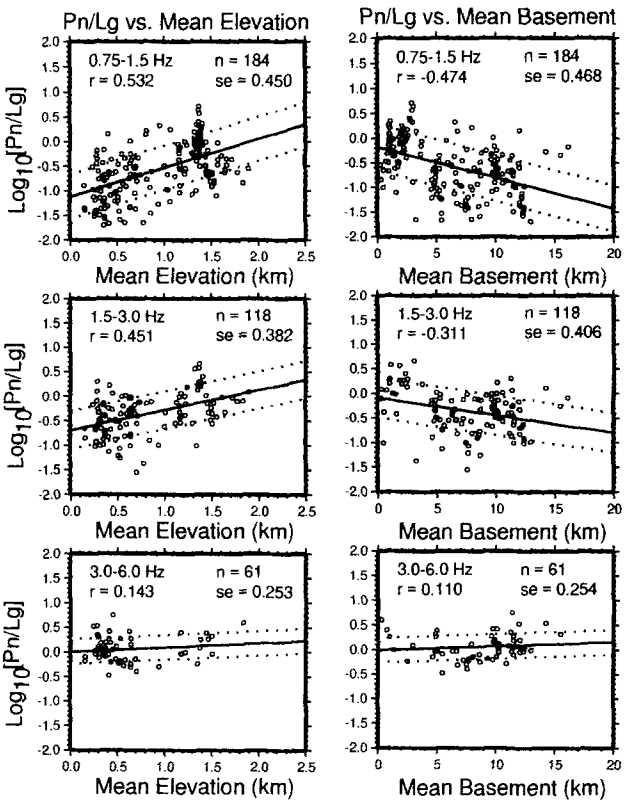

Figure 5. $\text{Log}_{10}[Pn/Lg]$ amplitude ratios for (*top*) 0.75 to 1.5 Hz, (*middle*) 1.5 to 3.0 Hz, and (*bottom*) 3.0 to 6.0 Hz versus along-path crustal wave-guide parameters: (a) mean elevation and (b) mean sediment thickness.

tions. In regions of sparse data coverage, the surface returns to an *a priori* background model. The error estimates associated with individual observations are propagated through the process resulting in a correction surface that accounts for measurement uncertainty. The surface is generated from the data and a few statistical parameters. More precisely, these parameters are (1) the correlation length, representing the spatial variability; (2) the background variance, representing the variability of the surface; and (3) the measurement error, representing the uncorrelated error in the measurements. In addition to these three parameters, the modified kriging algorithm also requires a blending range to determine how the surface is extrapolated in regions of sparse data coverage. These parameters are detailed in Schultz *et al.* (1998).

In order to choose the kriging parameters, it is necessary to characterize the statistical properties of the data. This is done by variogram modeling in standard kriging. We chose to plot the mean square differences of all pairs of observations as a function of the interpair distance. The raw observations are highly scattered, so we chose to bin the squared differences in 20-km-distance intervals and plot the mean values for all data within the bin. This is shown in Figure 7.

Table 2
Statistics of Cross-Validated Data Using Crustal Wave-Guide Regressions

Data Set	Number	Mean	σ	$\Delta\sigma$
Pn/Lg 0.75–1.5 data	184	−0.5622	0.5311	—
Pn/Lg 0.75–1.5 c-v	184	0.0186	0.4127	−22.3%
Pn/Lg 1.5–3.0 data	118	−0.3587	0.4276	—
Pn/Lg 1.5–3.0 c-v	118	−0.0200	0.3570	−16.5%
Pn/Lg 3.0–6.0 data	61	0.0620	0.2552	—
Pn/Lg 3.0–6.0 c-v	61	−0.0066	0.2436	−4.5%
Pg/Lg 0.75–1.5 data	201	−0.3178	0.3290	—
Pg/Lg 0.75–1.5 c-v	201	−0.0371	0.2420	−26.4%
Pg/Lg 1.5–3.0 data	153	−0.0538	0.2446	—
Pg/Lg 1.5–3.0 c-v	153	0.0313	0.1800	−26.4%
Pg/Lg 3.0–6.0 data	82	0.0833	0.1873	—
Pg/Lg 3.0–6.0 c-v	82	0.0288	0.1962	4.8%
Pn/Sn 0.75–1.5 data	183	−0.4047	0.4632	—
Pn/Sn 0.75–1.5 c-v	183	−0.0072	0.3636	−21.5%
Pn/Sn 1.5–3.0 data	123	−0.4838	0.4269	—
Pn/Sn 1.5–3.0 c-v	123	−0.0248	0.3404	−20.3%
Pn/Sn 3.0–6.0 data	70	−0.2884	0.3038	—
Pn/Sn 3.0–6.0 c-v	70	−0.0170	0.2502	−17.6%

Ratios are regressed on distance, mean elevation, rms elevation, mean basement depth, and mean Moho depth.
σ = root mean square, rms.
$\Delta\sigma$ = rms reduction of cross-validated data.
c-v = cross-validated data set using leave-one-out analysis.

The data are modeled by a simple analytic exponential function:

$$f(x) = b + c * [1.0 - \exp(-x/a)].$$

In the foregoing equation, $b = f(x = 0)$ is the measurement error (assuming the same measurement error exists for all data points), $b + c = f(x = \text{infinity})$ is the background variance, and a is the correlation length. The value of the mean squared difference for very large interpair distances, $b + c$, known in kriging literature as the sill value, represents the variance of the entire data set. For large interpair spacing, one does not expect the observation pairs to be correlated. The correlation model represents how quickly data pairs become relatively uncorrelated as the interpair spacing increases and approach the background variance. For the binned data plotted in Figure 7, it is apparent that a correlation length of 600 km, along with the intercept, $b = 0.1$, and multiplicative factor $c = 0.5$ represent the observations fairly well. We are most concerned with fitting the short wavelength behavior of the data. For large distances (>1000 km), no correlation is expected, and we are not distressed that the curve, $f(x; a = 600$ km), does not pass through the data points. Fortunately, kriging results are robust to changes in these statistical parameters, but it is, nonetheless, important to constrain these parameters by modeling the data.

Figure 6a shows the kriged surface for the *Pn/Lg* ratios (0.75 to 1.5 Hz) plotted with the individual observations. The mean of the data has been removed before kriging, so

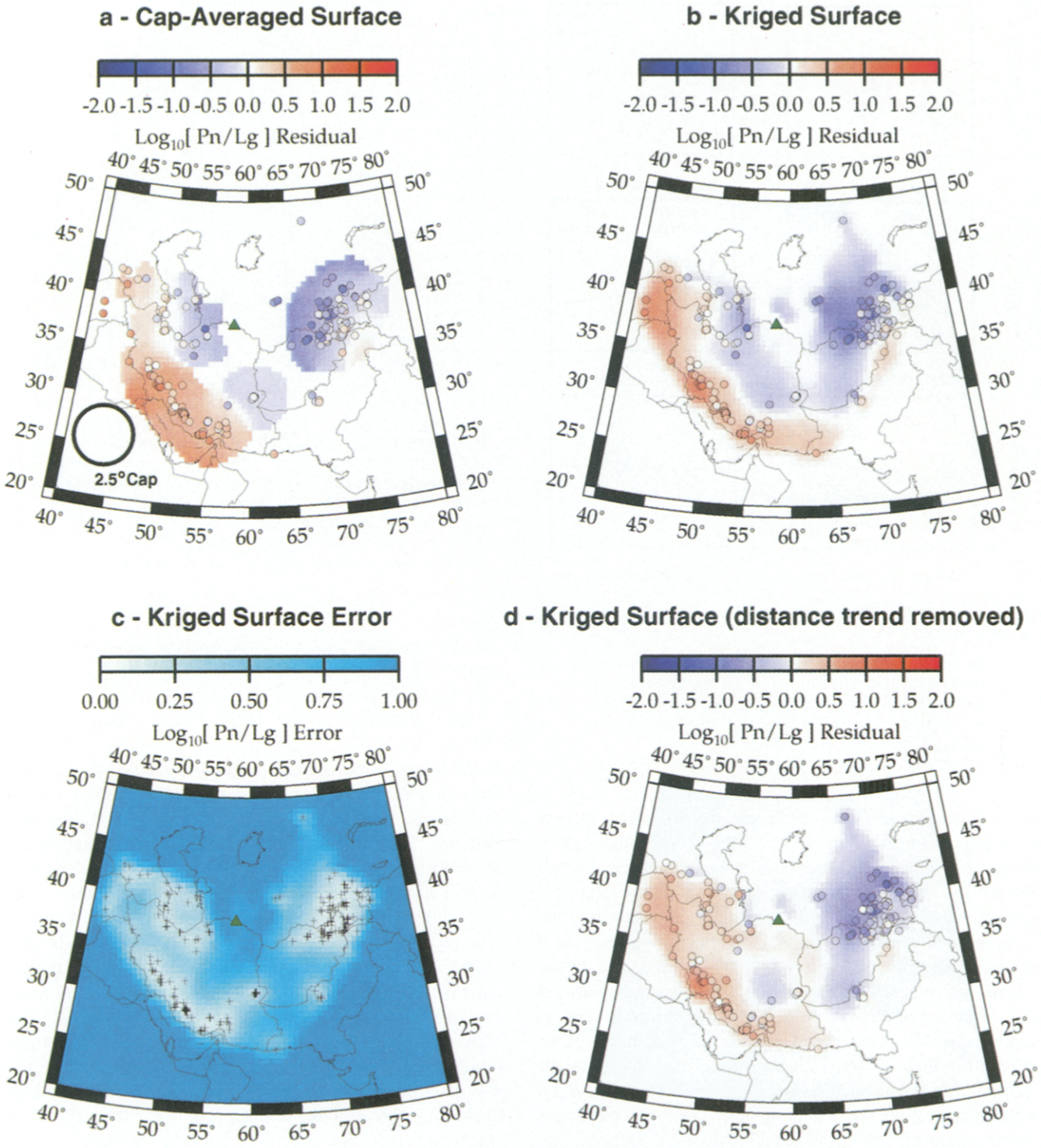

Figure 6. (a) Demeaned $Log_{10}[Pn/Lg]$ ratios for the passband 0.75 to 1.5 Hz (color-coded circles) plotted over the cap-average correction surface. The surface was computed on a 0.5° grid using a 2.5° radius cap and requiring at least five observations/cap. (b) Same $Log_{10}[Pn/Lg]$ ratios as (a) plotted over the kriged correction surface. Kriged surface was generated using a correlation length of 6.0°, blending range of 2.0°, background variance of 1.0 log units squared, and maximum measurement error of 0.2 log units squared. (c) Error surface for the kriged surface shown in (b). (d) Kriged surface for $Log_{10}[Pn/Lg]$ ratios 0.75 to 1.5 Hz after the distance trend shown in Figure 4a is removed.

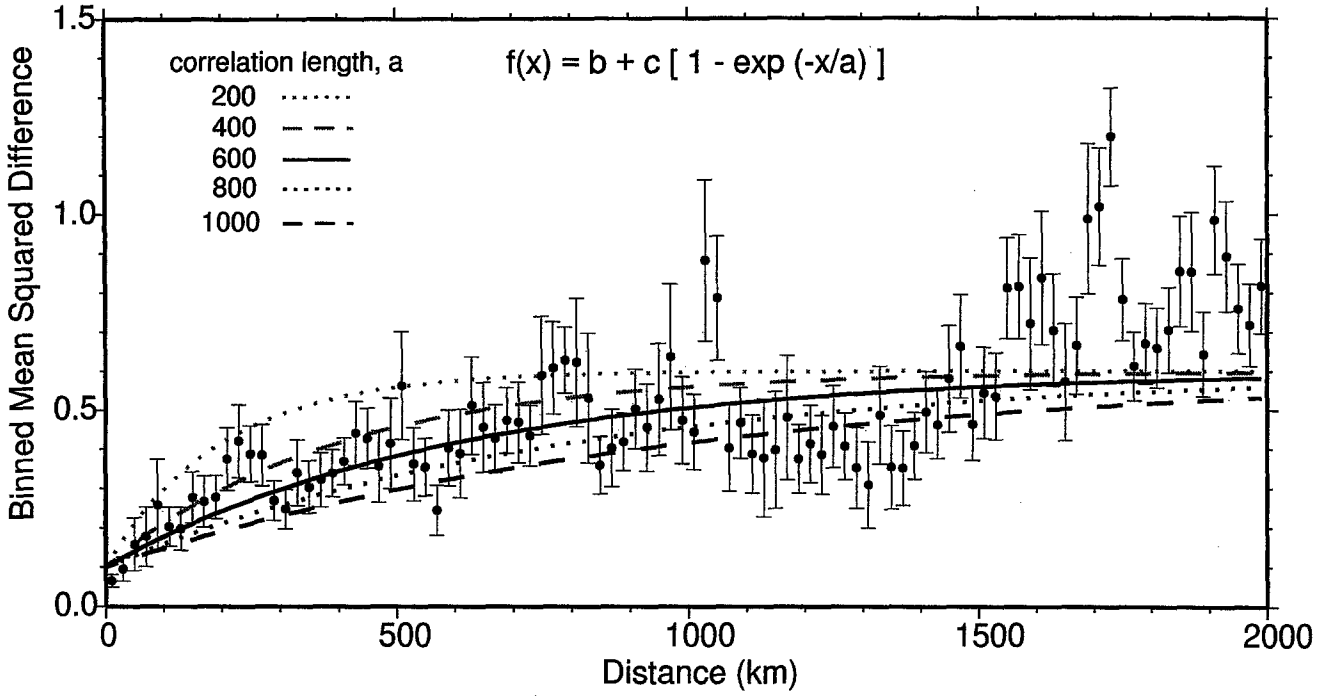

Figure 7. The binned mean squared difference of all pairs of $Log_{10}[Pn/Lg]$ ratios for the passband 0.75 to 1.5 Hz plotted versus the interpair distance. The data were binned into 20-km-distance bins, and the error bars represent 2-σ standard errors. The lines are exponential functions used to model the binned data.

corrections near zero correspond to the mean value of the entire data set. We chose a correlation length of 6.0°, a measurement error of 0.2 $\log_{10}[Pn/Lg]$ units, and background variance of 1.0 $\log_{10}[Pn/Lg]$ units. The kriged surface is defined only for points with distances from ABKT of 200 km or greater. Notice that the kriged surface follows the trends of the data more closely than the cap-averaged surface, especially on scales smaller than the cap radius (2.5°, Fig. 6a). In regions where the sampling is poor, the kriged surface returns to zero in a smooth fashion. The estimated error is plotted in Figure 6c. Notice that the error is small near data points but large (near the background variance) where the coverage is sparse. Thus, for a new event in a region of poor coverage, the kriged correction will be near the mean value of the data, and the estimated error will be large. However, corrections for new events in regions of good coverage will be near the local mean of the data with smaller error. Kriging does an excellent job of reducing the scatter in the observed *Pn/Lg* ratios. Cross-validation of the corrections derived with the kriging method reduces the rms by 46.7% and results in a more normally distributed population shown in Figure 4e.

The pattern of the correction surface plotted in Figure 6b appears to have a distance trend. That is, events on the periphery of the sampled region tend to have high ratios compared to events closer to ABKT. As shown in Figure 3a, the low-frequency *Pn/Lg* ratios have a positive slope distance trend. We removed this trend and kriged the residual amplitude ratios, shown in Figure 6d. These residuals and the associated correction surface show a larger scale pattern of positive and negative values. The error surface for this case is similar to that shown in Figure 6c. Cross-validation of the data using this approach resulted in a slightly larger rms reduction (49.1%, Fig. 4f) than the kriging method without removing the distance trend. An important effect of removing the distance trend is that the background model used for determining the residual amplitude ratios for kriging is probably more appropriate than simply demeaning the data before kriging.

Discussion

Short-period regional *P/S* ratios hold much promise for identifying low-magnitude seismic events. However, path propagation effects lead to variability in the *P/S* ratios that can inhibit isolation of the seismic source. The regional *P/S* observations presented earlier show great variability due to path effects. In this article, we investigated four strategies for representing path propagation effects on regional *P/S* discriminants. While each strategy succeeds in reducing the discriminant scatter, the kriging method provides the greatest scatter reduction (Fig. 4) and has several advantages that distinguish it from the other methods. In the following sections, we discuss the results along with the features and shortcomings of each method. The advantages and disadvantages of each method are summarized in Table 3. Finally,

Table 3
Summary Comparison of Methodologies

Method	Advantages	Disadvantages
Sector/distance	works well	discontinuous difficult to draw boundaries
Path parameter regression	continuous	does not work very well crustal wave guide not well known
Cap averaging	works well easy to compute	poorly defined error surface undefined where data are sparse
Kriging	works best continuous well-defined error	computationally intensive

we discuss the more general applicability of these results to regional seismic discrimination.

Distance Corrections

Distance corrections have a well-founded theoretical justification because geometric spreading and attenuation lead directly to a distance dependence for ratios of regional *P*- and *S*-wave phase amplitudes. For regions where elastic and anelastic structure are approximately constant, it is expected that *P/S* ratios vary most strongly with distance. The *Pn/Lg*, *Pg/Lg*, and *Pn/Sn* ratios observed at ABKT are highly scattered and show only a weak dependence on distance when data from all azimuths are grouped together. This observation alone indicates that path propagation effects due to laterally varying structure are important for the *P/S* ratios recorded at ABKT. However, when the data are subdivided by azimuth to isolate distinct source regions and path properties, the distance trends are stronger (Fig. 3). The case of ABKT is unique because this station is situated near a major tectonic boundary, so paths from different azimuths sample completely different crustal structures. This point is clearly illustrated in Rodgers *et al.* (1997d, Fig. 4). It is interesting to contrast the distance trends for data from all azimuths at ABKT with the *P/S* ratios observed at WMQ and reported by Lay *et al.* (1997). That study shows that *P/S* ratios at WMQ are more strongly correlated with distance than the ABKT data set presented here, suggesting that propagation effects due to laterally varying structure are less important at WMQ or that distance is correlated with other parameters that control the *P/S* amplitude behavior. The WMQ paths do show correlation of distance with mean elevation, rms elevation, mean Moho depth, and mean sediment depth (Fan and Lay, 1998a). So in the case of WMQ, distance corrections may be successful because of covariance between path characteristics. Although the sectorized distance corrections significantly reduce the scatter of the *P/S* ratios observed at ABKT, there are certain problems that can arise with this method. If a tectonic region is poorly defined or aseismic, then it may be difficult to define the sector boundaries. If tectonic boundaries are oblique to great-circle paths of regional events to a given station, then azimuthal sectorization may not succeed in reducing *P/S* ratio scatter. Because of uncertainties in event location (typically less than 30 km), one must be cautious when associating an event with a sector when the event is near the sector boundary. It is probable that the corrections do not vary smoothly across a sector boundary, which is an undesirable feature of the sectorization method. Finally, the only way to assess the uncertainty in a distance correction is from the formal errors of the regression, which will not represent the true uncertainty if the data are not Gaussian distributed.

Path-Specific Crustal Wave-Guide Corrections

Regressions of *P/S* discriminants on path-specific crustal wave-guide parameters provide a continuous parameterization of the data, and they succeed in reducing the observed scatter. However, the rms reductions are not as significant as the other methodologies. The fact that certain wave-guide properties are better predictors of *P/S* behavior than distance alone supports the azimuthal sectorization strategy presented earlier and in Rodgers *et al.* (1998d). Crustal wave-guide parameter regression studies report that *P/S* ratios behave differently at each station, so that corrections derived for one region may not be transportable to another region. For example, the univariate regression parameters reported by Fan and Lay (1998a) for *P/S* ratios observed at WMQ are different from the values obtained by regressing *P/S* ratios observed at ABKT. However, the slopes of the trends are generally in agreement (e.g., low-frequency *P/S* ratios are positively correlated with distance, mean elevation, and mean crustal thickness, and negatively correlated with mean sediment thickness). This issue is investigated further in the multiple-station path parameter regression analysis reported by Fan and Lay (1998c). It is possible that scatter reductions result because the path-specific parameters are surrogates for the true controlling factors, and there are correlations between the parameters chosen and the true controlling factors, similar to the covariance between distance and other path parameters at WMQ discussed in the last section. Another important issue that arises when employing this technique is the fact that models of sediment and Moho depth are either poorly constrained or completely unknown.

Cap Averaging

Cap averaging is a straightforward spatial averaging technique that results in a substantial reduction of the *P/S* discriminant scatter. The method is easy to apply to any data set and does not require models of crustal structure. For densely sampled, smoothly varying data sets, this technique may provide an excellent representation of the data. However, for the realistic seismic amplitude data sets we considered in this study, cap averaging has a few disadvantages that severely limit its applicability. Cap averaging provides no error estimate, other than the standard error of the mean

or the actual spread of the data within each cap. Cap averaging cannot represent data that varies on spatial scales smaller than the cap radius, as discussed previously. Also, no model prediction is obtained for poorly sampled or aseismic regions. Modifications could be made to force the surface to return to background model, along the lines of modified kriging; however, the above-stated limitation regarding error estimates would remain.

Modified Kriging

Modified kriging provides an excellent representation of the *P/S* ratio data observed at ABKT and has several important features that distinguish it from the other representation methodologies. Kriging provides the largest rms reduction and the corrected low-frequency *Pn/Lg* ratios (Figs. 4e and 4f) are very nearly normally distributed. Kriging results in a continuous correction surface for all points in a specified region and returns smoothly to an *a priori* background model in sparsely sampled regions. An error estimate exists at each point based on data measurement error and other statistical properties of the data. Small-scale variability is better represented by kriging than by cap averaging (see Figs. 6a and 6b) because cap averaging is a low-pass filter. Spatial wavelengths of the kriged correction surface are controlled by the data and the kriging parameters described earlier. Identified regions that block *S*-wave phases (*Sn* or *Lg*) can easily be incorporated into the kriged surfaces so that if a path is expected to have a blocked *S* wave, the correction will be flagged and the *Sn* or *Lg* amplitude will not be used to form a discriminant. In Figure 6d, the *P/S* ratios were preprocessed to remove the distance trend, then the resulting residual ratios were kriged. It is worth noting that the data can be preprocessed using any of the methodologies presented here, and the residual amplitude ratios can be kriged. For example, Phillips (1999) corrected *P/S* ratios for a path parameter regression model before kriging the residual amplitude ratios. Similarly, absolute amplitudes can be preprocessed by removing corrections based on an attenuation tomography map or on the source and path-corrected amplitudes (Taylor and Hartse, 1998). A possible disadvantage of the kriging technique is that it is computationally intensive relative to the other methods. However, given the speed of modern computers and the significant advantages of kriging over other methods, the longer run time of this method relative to others should not limit its use. The most important issue regarding speed is the ability to retrieve the correction in a real-time monitoring situation. This can be done rapidly once the correction surface is defined.

General Comments

The path-correction strategies presented here reduce the scatter in the low-frequency (<3.0 Hz) *P/S* amplitude ratios, while not significantly reducing the scatter in the higher frequencies in a consistent fashion. Similar results were reported by Fan and Lay (1998a,b) and Rodgers *et al.* (1997b). Many studies have reported that higher frequency *P/S* ratios discriminate better than lower frequency *P/S* ratios (e.g., Walter *et al.*, 1995; Taylor, 1996). However, strong lithospheric attenuation can significantly reduce the signal-to-noise ratio in the higher frequency bands for the smaller events ($m_b < 4.5$) at distances of 500 km or more that are of particular concern to the CTBT monitoring effort. It is possible that for such events there will not be sufficient signal to noise to measure *P/S* ratios at frequencies above 3.0 Hz. Thus, if the strategies presented here can reduce the scatter in the low-frequency *P/S* ratios, they may enhance discrimination capabilities. Unfortunately, we cannot ensure that reducing the scatter in low-frequency *P/S* ratios will improve discrimination. We have included all paths for which the phase amplitude signal-to-pre-*Pn*-noise is greater than 2.0. It is certainly possible that we have included paths for which *Sn* or *Lg* are weak or blocked, given previous studies of regional-phase behavior (Kadinsky-Cade *et al.*, 1981; Rodgers *et al.*, 1997a). The low-frequency *Pn/Lg* ratios show a continuous distribution (e.g., Fig. 4a), suggesting that blockage cannot be easily identified by a maximum *P/S* ratio. However, if blockage and attenuation are complete, blocked paths cannot be used for source discrimination. If paths with weak or absent *S*-wave energy were discarded, then the variability would be reduced and variance reductions might not be as strong. The representations presented here certainly describe the expected earthquake *P/S* behavior, including paths for which *Sn* or *Lg* is partially or totally blocked. So at the very least, the analysis presented here helps us understand the regional-phase behavior and predict the earthquake *P/S* ratios recorded at ABKT. We are currently investigating techniques to separately map regions of *Sn* and *Lg* blockage. Once these regions are identified, they can be incorporated into the correction surfaces. The test of whether variance reductions of earthquake measurements improves discriminant performance in this region requires explosion data. We are currently looking for evidence of mining explosions recorded at ABKT. The acquisition of waveform data recorded at ABKT for explosion sources at regional distances will allow us to investigate if path corrections enhance seismic source discrimination.

Acknowledgments

Raw waveform data were obtained from the Incorporated Research Institutions for Seismology–Data Management Center (IRIS-DMC). Data were collected and organized by Stan Ruppert and Terri Hauk. Data were processed using SAC2000 developed by the Lawrence Livermore National Laboratory. Figures were made using the GMT3.0 software package (Wessel and Smith, 1991). We are grateful to Dogan Seeber and Mauwia Barazangi of Cornell University for providing the Former Soviet Union Institute of Physics of the Earth basement and Moho depth models. We are grateful to Guanwei Fan for assistance with the multivariate regression analysis. We thank Scott Phillips, Hans Hartse, and Steve Taylor for sending us articles prior to publication. Editorial comments from Anton Dainty and reviews by Doug Baumgardt and Mark Fisk improved the text. Research was performed under the auspices of the U.S. Department of Energy by the Lawrence Livermore National Laboratory under Contract W-7405-ENG-48. This is LLNL Journal Contribution UCRL-JC-131035. Contribu-

tion Number 356, University of California Santa Cruz Institute of Tectonics.

References

Baumgardt, D. (1990). Investigation of teleseismic Lg blockage and scattering using regional arrays, *Bull. Seism. Soc. Am.* **80,** 2261–2281.

Baumgardt, D. (1996). Investigation of Lg blockage and the transportability of regional discriminants in the Middle East, Scientific Report No. 1, PL-TR-96-2294, 11 November 1996, ENSCO Inc., Springfield, Virginia.

Baumgardt, D. and C. Schneider (1997). Multivariate canonical correlations of P/S ratios and propagation path parameters for Iran, *Proc. of the 19th Annual Seismic Research Symposium on Monitoring a Comprehensive Test Ban Treaty,* 23–25 1997, Defense Special Weapons Agency Report, 14–23.

Baumgardt, D. and G. Young (1990). Regional seismic waveform discriminants and case-based event identification using regional arrays, *Bull. Seism. Soc. Am.* **80,** 1874–1892.

Bennett, T. and J. Murphy (1986). Analysis of seismic discrimination capabilities using regional data from western United States events, *Bull. Seism. Soc. Am.* **76,** 1069–1086.

Blandford, R. (1981). Seismic discrimination problems at regional distances, in *Identification of Seismic Sources—Earthquake or Explosion,* E. Husebye and S. Mykkeltveit (Editors), Reidel, Boston, 695–740.

Fan, G. and T. Lay (1998a). Statistical analysis of irregular waveguide influences on regional seismic discriminants in China, *Bull. Seism. Soc. Am.* **88,** 74–88.

Fan, G. and T. Lay (1998b). Statistical analysis of irregular waveguide influences on regional discriminants in China: additional results for Pn/Sn, Pn/Lg, and Pg/Sn, *Bull. Seism. Soc. Am.* **88,** 1504–1510.

Fan, G. and T. Lay (1998c). Regionalized versus single-station waveguide effects on seismic discriminants in western China, *Bull. Seism. Soc. Am.* **88,** 1260–1274.

Hartse, H., S. Taylor, S. Phillips, and G. Randall (1997). A preliminary study of regional seismic discrimination in Central Asia with emphasis on western China, *Bull. Seism. Soc. Am.* **87,** 551–568.

Hartse, H., R. Flores, and P. Johnson (1998). Correcting regional seismic discriminants for path effects in western China, *Bull. Seism. Soc. Am.* **88,** 596–608.

Hearn, T. and J. Ni (1994). Pn velocities beneath continental collision zones: the Turkish–Iranian plateau, *Geophys. J. Int.* **117,** 273–283.

Kadinsky-Cade, K., M. Barazangi, J. Oliver, and B. Issacks (1981). Lateral variations of high-frequency seismic wave propagation at regional distances across the Turkish and Iranian plateaus, *J. Geophys. Res.* **86,** 9377–9396.

Kim, W.-Y., D. Simpson, and P. Richards (1993). Discrimination of earthquakes and explosions in the eastern United States using high-frequency data, *Geophys. Res. Lett.* **20,** 1507–1510.

Kunin, N. (1987). Distribution of sedimentary basins of Eurasia and the volume of the Earth's sedimentosphere, *Int. Geol. Rev.* **22,** 1257–1264.

Kunin, N. and E. Sheykh-Zade (1983). New data on lateral inhomogeneities in the upper mantle under western Eurasia, *Dokl. Akad. Nauk. USSR* **273,** 1087–1091.

Lay, T., G. Fan, and A. Rodgers (1997). Crustal waveguide effects on regional phases in China and Southeast Asia, Phillips Laboratory Report PL-TR-97-2163, Hanscom AFB, Massachusetts.

Mitchell, B., Y. Pan, J. Xie, and L. Cong (1997). Lg coda Q variations across Eurasia and its relation to crustal evolution, *J. Geophys. Res.* **102,** 22767–22779.

National Research Council (1997). Research required to support comprehensive nuclear test ban treaty monitoring, National Academy Press, Washington, D.C., 138 pp.

Phillips, W. S. (1999). Empirical path corrections for regional-phase amplitudes, *Bull. Seism. Soc. Am.* **89,** 384–393.

Phillips, W. S., G. Randall, and S. Taylor (1998). Path correction using interpolated amplitude residuals: an example from central China, *Geophys. Res. Lett.* **25,** 2729–2732.

Pomeroy, P., J. Best, and T. McEvilly (1982). Test ban treaty verification with regional data—a review, *Bull. Seism. Soc. Am.* **72,** S89–S129.

Rodgers, A., J. Ni, and T. Hearn (1997a). Propagation characteristics of short-period Sn and Lg in the Middle East, *Bull. Seism. Soc. Am.* **87,** 396–413.

Rodgers, A., T. Lay, G. Fan, and W. Walter (1997b). Calibration of distance and path effects on regional P/S discriminants at station ABKT (Alibek, Turkmenistan): statistical analysis of crustal waveguide effects, UCRL-JC-129165.

Rodgers, A., T. Lay, W. Walter, and K. Mayeda (1997c). Comparison of regional phase amplitude ratio measurement techniques, *Bull. Seism. Soc. Am.* **87,** 1613–1621.

Rodgers, A., W. Walter, and T. Lay (1997d). Calibration of distance and path effects on regional P/S discriminants at station ABKT (Alibek, Turkmenistan): azimuthal sector regionalization, UCRL-JC-128318.

Schultz, C, S. Myers, J. Hipp, and C. Young (1998). Nonstationary Bayesian kriging: application of spatial corrections to improve seismic detection, location and identification, *Bull. Seism. Soc. Am.* **88,** 1275–1288.

Seber, D., M. Vallve, E. Sandvol, D. Steer, and M. Barazangi (1997). Middle East tectonics: applications of geographical information systems (GIS), *GSA Today,* February 1997, 1–5.

Taylor, S. (1996). Analysis of high-frequency Pg/Lg ratios from NTS explosions and western U.S. earthquakes, *Bull. Seism. Soc. Am.* **86,** 1042–1053.

Taylor, S. and H. Hartse (1998). A procedure for estimation of source and propagation corrections for regional seismic discriminants, *J. Geophys. Res.* **103,** 2781–2789.

Taylor, S., M. Denny, E. Vergino, and R. Glasner (1989). Regional discrimination between NTS explosions and western U.S. earthquakes, *Bull. Seism. Soc. Am.* **79,** 1142–1176.

Walter, W., K. Mayeda, and H. Patton (1995). Phase and spectral ratio discrimination between NTS earthquakes and explosions. Part I: empirical observations, *Bull. Seism. Soc. Am.* **85,** 1050–1067.

Wessel, P. and W. Smith (1991). Free software helps map and display data, *EOS* **72,** 445–446.

Zhang, T.-R. and T. Lay (1994a). Analysis of short-period regional phase path effects associated with topography in Eurasia, *Bull. Seism. Soc. Am.* **84,** 119–132.

Zhang, T.-R. and T. Lay (1994b). Effects of crustal structure under the Barents and Kara Seas on short-period regional wave propagation for Novaya Zemlya explosions: empirical relations, *Bull. Seism. Soc. Am.* **84,** 1132–1147.

Zhang, T.-R., S. Schwartz, and T. Lay (1994). Multivariate analysis of waveguide effects on short-period regional wave propagation in Eurasia and its application in seismic discrimination, *J. Geophys. Res.* **99,** 21929–21945.

Zhang, T.-R., T. Lay, S. Schwartz, and W. Walter (1996). Variation of regional seismic discriminants with surface topographic roughness in the western United States, *Bull. Seism. Soc. Am.* **86,** 714–725.

Geophysics and Global Security Division,
Lawrence Livermore National Laboratory
Livermore, California 94551
(A.J.R., W.R.W., C.A.S., S.C.M.)

Institute of Tectonics and Earth Sciences Department
University of California
Santa Cruz, California 95064
(T.L.)

Manuscript received 11 July 1998.